NUCL SCI TECH (2018) 29:57
https://doi.org/10.1007/s41365-018-0386-0

Cross-sectional investigation of radiation damage of 2 MeV proton-irradiated silicon carbide

Xu Wang[1] · Yan-Wen Zhang[2] · Dong Han[3] · Yun-Biao Zhao[3] · Zi-Qiang Zhao[3] · Ming Zhang[1]

Received: 12 April 2017 / Revised: 29 June 2017 / Accepted: 7 July 2017 / Published online: 19 March 2018

Abstract Cross-sectional investigation is an important method to study ion irradiation effects in the depth direction. In this study, 2 MeV H^+ was implanted in 6H-SiC single crystals to investigate the effects of light ion irradiation on SiC. Raman spectroscopy and scanning electronic microscopy (SEM) were carried out on cross-sectional samples to reveal the in-depth damage states and dopant behavior. The most damaged region is a little shallower than that predicted by the SRIM procedure, owing to the uncertainty in SRIM simulations. Layered structures representing zones of varying damage after 2 MeV H ion irradiation are clearly observed. Two bands are observed in SEM images, of which on band corresponds to the damage peak, while the other band at the end of the H ion-affected area is probably a result of H diffusion propelled by a hydrogen-rich layer during irradiation. A charge accumulation effect related with conductivity on the sample surfaces during SEM tests is observed in the H-implanted area. A model is proposed to explain these phenomena.

Keywords SiC · Proton irradiation · Cross-sectional analysis · Raman spectroscopy · SEM

1 Introduction

Silicon carbide (SiC) is of scientific and technological interest for its potential applications in nuclear energy systems. It is also an attractive wide band-gap semiconductor for a broad range of applications such as high-frequency, high-power, and high-temperature devices [1, 2]. Understanding the effects of energetic ion irradiation on SiC is therefore desirable. In particular, irradiation from light ions like H as well as its diffusion behavior needs further investigation. Proton implantation-induced defects in SiC and the related electrical properties have been extensively investigated [3–10]. Hydrogen has been found to be mobile at low temperatures and can diffuse at a μm scale in p-type SiC, while no such effect has been found in n-type samples [11]. On the other hand, H ion irradiation has been found to generate radiation damage defects, which are known to trap hydrogen very effectively, reducing its mobility [12]. In turn, this influences the irradiation effects. Additionally, high-energy light ion implantation, like MeV protons implanted in SiC, will result in a large penetration depth. The discrepancies in radiation damage and dopant profiles between experimental observations and classic Stopping and Range of Ions in Matter (SRIM) code [13] predictions are of interest. Thus, more attention should be paid to the high-energy proton-induced damage states as a function of depth and impurity/dopant behavior in SiC.

This work was supported by the National Natural Science Foundation of China (Grant Nos. 11705169, 91426304 and 91226202).

✉ Xu Wang
xuwang89@caep.cn

✉ Zi-Qiang Zhao
zqzhao@pku.edu.cn

[1] Institute of Materials, China Academy of Engineering Physics, Jiangyou 621908, China

[2] Department of Nuclear Physics, China Institute of Atomic Energy, Beijing 102413, China

[3] State Key Laboratory of Nuclear Physics and Technology, Institute of Heavy Ion Physics, School of Physics, Peking University, Beijing 100871, China

In this work, 2 MeV H^+ irradiation was carried out to investigate in-depth radiation damage and the dopant behavior of high-energy light ions implanted in SiC. Investigation on cross-sectional samples is a good methodology for probing large perturbed depth, which has been reported in [14–18]. The combined use of Raman spectroscopy and scanning electronic microscopy (SEM) allows one to study the irradiation effects and discrepancies between experimental results and SRIM calculations. A model has been proposed to elucidate the layered structures observed in the range of H ions in SiC.

2 Experimental

2 MeV H^+ was implanted into n-type single crystal 6H-SiC(0001) wafers at a fluence of 2.7×10^{17} cm^{-2}. Two samples were polished to a mirror-like finish by chemical mechanical polishing and reconstituted to limit radiative losses from the analyzed surface during irradiation [16]. The ion implantation was performed at an angle of 7° to avoid channeling effects using a 4.5 MV electrostatic accelerator at Peking University at room temperature (RT). The damage in terms of displacement per atom (dpa) and the depth distribution of H atoms according to the classic Monte Carlo simulations by SRIM are depicted in Fig. 1a. The threshold displacement energies used for C and Si sublattices are 20 and 35 eV, respectively [19]. It is seen that the Bragg peak is very obvious for light ions like H^+ and the hydrogen concentration is about 2.0 at.%.

After irradiation, the Raman (Horiba J.Y. LabRAM ARAMIS) and SEM (FEI NanoSEM 430) analyses were carried out to investigate the disorder profile and the range of H ions. Figure 1b shows a schematic diagram of cross-sectional investigation by Raman and SEM. Raman spectroscopy has been proved to be effective in the study of cross sections of ion-irradiated samples [14–18]. The depth dependence of damage induced by ion irradiation was evaluated by Raman line scan measurements. The Raman spectra were obtained with a 1800 lines/mm grating using a laser wavelength of 532 nm with a scanning range of 600–1200 cm^{-1} at a spectral resolution of 0.8 cm^{-1} at RT. A 100× objective with a numerical aperture of 0.9 was employed during the Raman tests. Raman spectroscopy has a depth resolution at about 1 μm and is sensitive to disorders induced in SiC by ion irradiation. Furthermore, the cross-sectional surface of our sample was analyzed by SEM to reveal the structures affected by ion implantation in depth. SEM was used as a complementary technique to investigate the distribution of H ions and the corresponding damage. The results are compared with SRIM calculations.

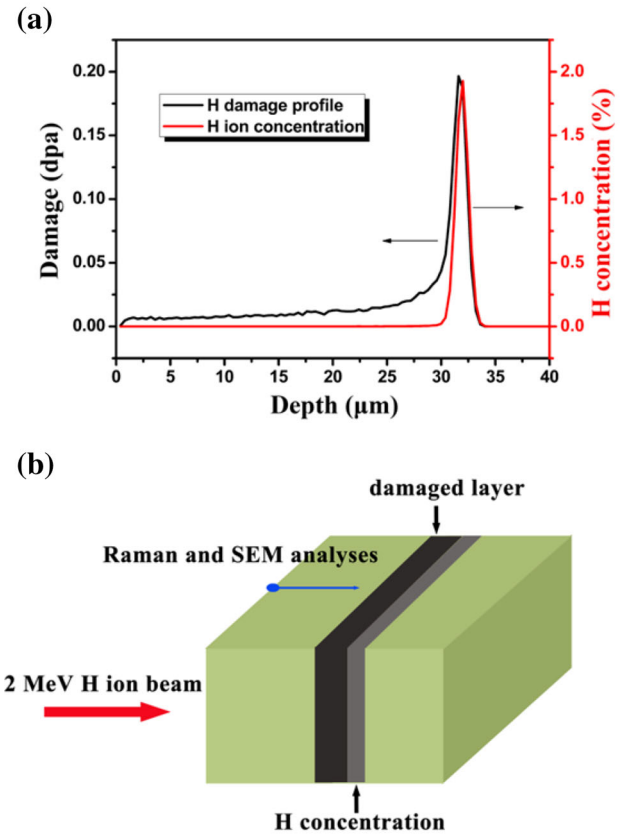

Fig. 1 (Color online) **a** Depth distribution of H ions and dpa profile (for a fluence of 2.7×10^{17} cm^{-2}); **b** schematic diagram of cross-sectional investigation by Raman and SEM

3 Results and discussion

Figure 2a shows typical Raman spectra recorded along the ion implantation path. The incident surface is marked as 0 μm. The characteristic peaks of 6H-SiC, which are usually used as indicators of damage level, and the related defect types are evolved with the depth, as shown in Fig. 2a. Figure 2a also shows that the most damaged region is around 29.5 μm deep and this area is almost amorphous. At a depth of 40 μm, the presence of crystalline SiC is confirmed. A little disorder is observed at the surface of the 2 MeV H^+-implanted SiC, as illustrated in Fig. 2b. The Raman spectra of the boundary (0 μm), the most damaged area (29.5 μm), the unaffected area (by H ions, 40 μm) and the two transition states between 0 and 29.5 μm (15 μm chosen) and 29.5 and 40 μm (35 μm chosen) are depicted in Fig. 2c–g. The damage level increases as the Raman intensity decreases at a depth of 15 μm, as shown in Fig. 2d. Signals indicating disordered/distorted or amorphous Si–C are observed in the most damaged region, as shown in Fig. 2e, which is in accordance with [20]. From 35 μm, which is beyond the damage peak, the Raman intensity increases drastically until the undamaged region

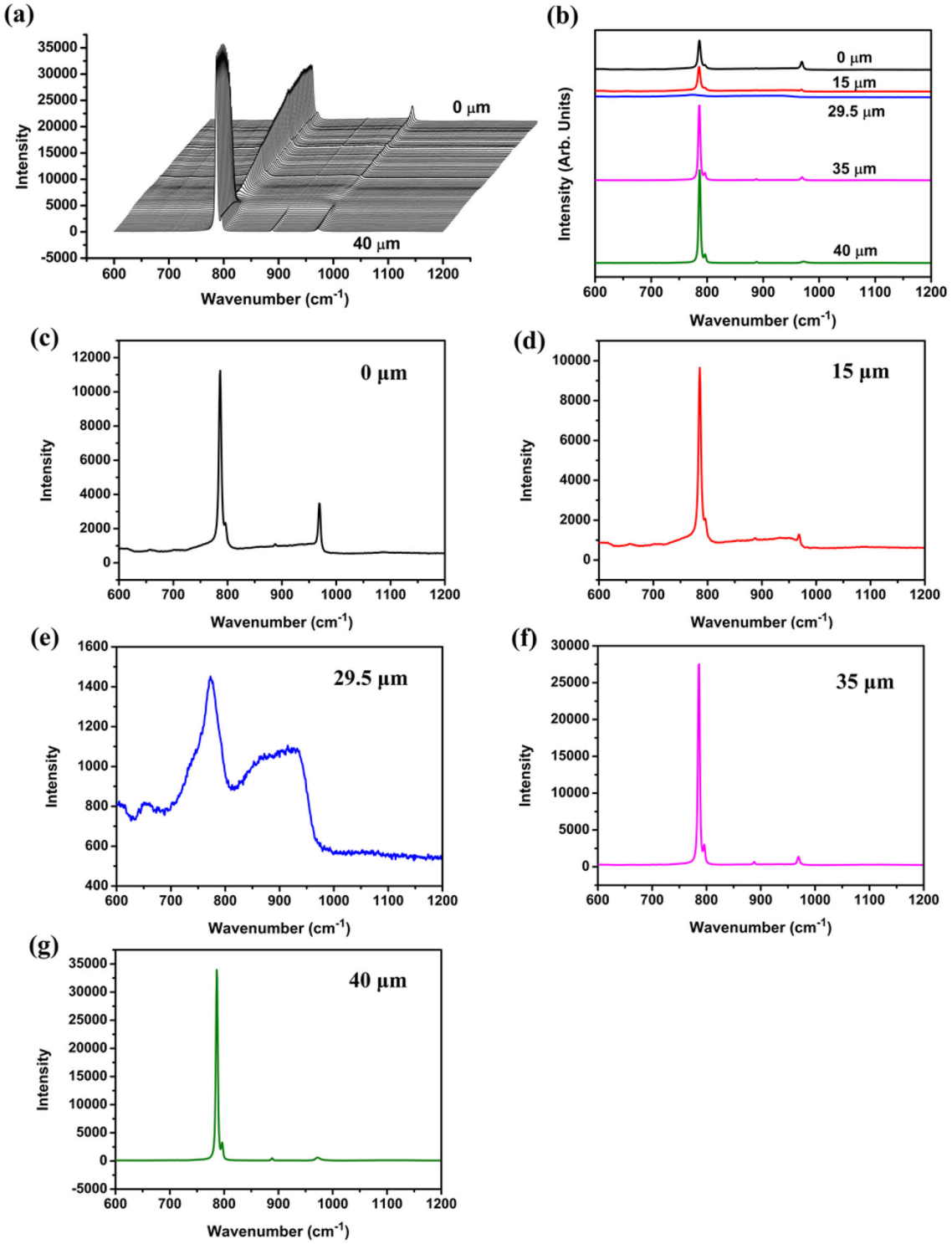

Fig. 2 (Color online) Raman line scan measurements **a** performed at RT on the cross section of the irradiated sample; **b** Raman spectra of 2 MeV H ion-irradiated SiC at 0, 15, 29.5, 35 and 40 μm, and the figures of separate curves (**c**)–(**g**)

(40 μm). It can be seen that 2 MeV H ion-induced damage is highly heterogeneous in the implantation direction. The present cross-sectional study is applicable for deep penetration depth (several or tens of micrometers) due to the MeV H^+ energy. Although the evolution of Raman intensity with depth is not a direct representation of damage evolution, Raman line scan measurements can depict the damage profile approximately and conveniently.

In order to elucidate the damage profile of 2 MeV H ion-irradiated SiC, a characteristic Raman peak of our sample is further investigated. Figure 3a, b presents the peak position and the width of the A_1 (TO) mode at 787 cm^{-1} as a function of depth. The width was measured by full width at half maximum. It is seen that the peak position moves to lower wavenumbers as the damage increases from the surface to the most damaged region. Concurrently, the width increases, which is an agreement with our previous work [15]. The evolution of the relative area (RA) with implantation depth is shown in Fig. 3c. The RA is an indication of damage level, derived by the area of the A_1 (TO) mode at 787 cm^{-1} obtained from deconvolution and normalized to the value of pristine SiC. Figure 3c shows that the region of most damage is around 29.5 μm, slightly shallower than that of SRIM simulations (31.6 μm). The RA of the boundary area is about 0.4, indicating a relatively low damage induced by H^+ irradiation near the ion implantation surface. Figure 3c shows that the area affected by H ions extends as deep as ~ 36 μm, corresponding to an RA value of about 1.0 at that depth. The steep curve of RA, which corresponds to the drastically reduced implantation damage, shows that some of the implanted H ions will still move beyond the most damaged region until they completely stop. The effect of the H ions extended to depths greater than those simulated by SRIM (see Fig. 1a). Therefore, it can be concluded that the stragglings of the simulated hydrogen and vacancy distributions are lower than in reality. Besides, the SRIM code does not account for diffusion of defects and hydrogen ions, which may affect the resulting damage profile.

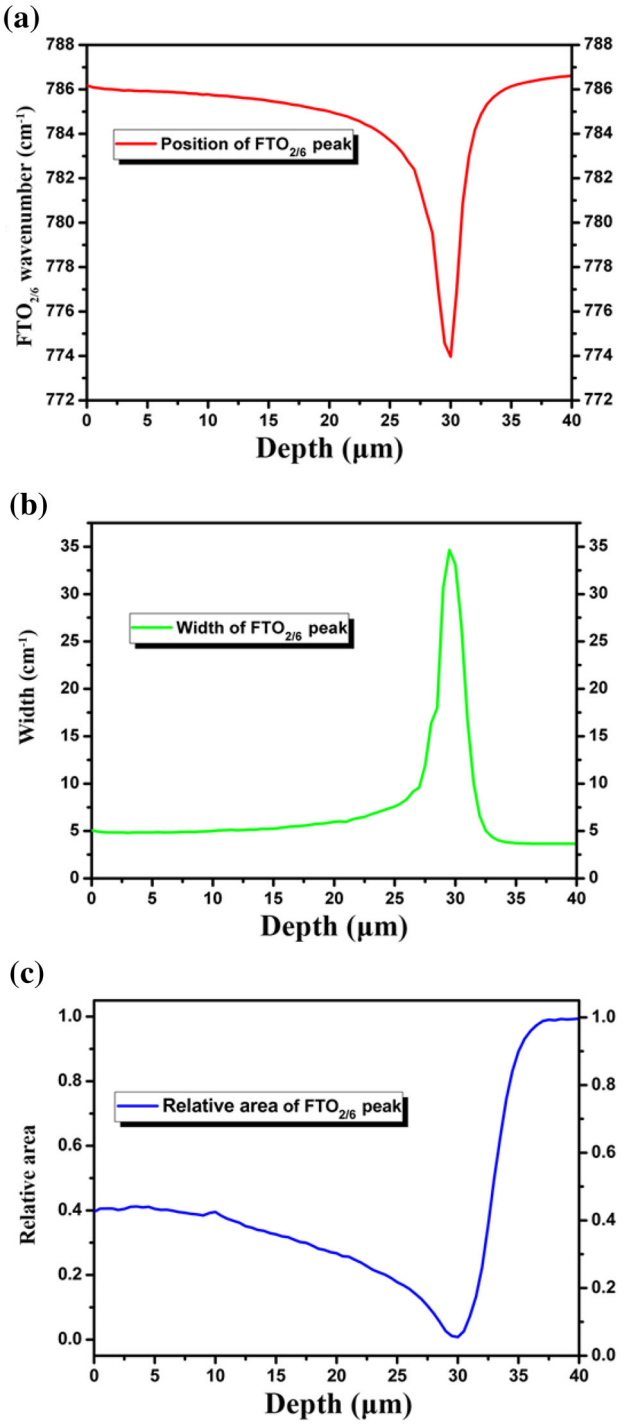

Fig. 3 (Color online) The depth evolution of the A_1 (TO) peak position (**a**) and width (**b**) of the sample. (**c**) The RA of the A_1 (TO) mode area at 787 cm^{-1} as a function of depth

The frequency shift and width evolution of the $FTO_{2/6}$ peak with depth plotted in Fig. 3a, b are related to the damage formation and the resulting strains [15]. It is worth noting that the damage peak estimated by numerical SRIM calculation of 2 MeV H^+ was 32 μm, which is in close agreement with the results obtained from Raman measurements. However, some discrepancies exist. These discrepancies can be explained by the inaccurate estimation of energy loss, either nuclear or electronic, in SRIM code, which can be ascribed to an underestimation of the stopping power calculated by SRIM, resulting in an overestimation of the depth of the damage peak.

Lindhard et al. developed the equation to predict the ion range based on the measured electronic stopping power [21]

$$R_p = \frac{R}{1 + (M_2/3M_1)}, \tag{1}$$

where $M_1(1)$ and $M_2(20)$ are the mass of the implanted ions and the target, respectively. The total ion path, R, can be obtained by the formula

$$R = \frac{1}{N}\int_0^{E_i} \frac{dE}{[S_n(E) + S_e(E)]}, \tag{2}$$

where $S_n(E)$, $S_e(E)$, E_i and N are the nuclear and electronic stopping power, the incident energy, and the density of the target, respectively. The damage profile will be

proportional to ion range distribution. Thus, the discrepancy observed in the present case is conjectured to result from an underestimation of stopping power.

It is possible that the stopping power is increased owing to the synergistic effects of nuclear and electronic energy. Several investigations have found overestimated electronic stopping power for heavy ions like Au and Pt in light targets [22–26]. Although the SRIM predictions have a good agreement for light ions [27–29], a slight underestimation of the stopping power in SRIM can be inferred in the present case. Efforts have been made to investigate the stopping power both theoretically and experimentally [30–32], with results showing that discrepancies exist.

In general, SRIM provides a good evaluation of the spread of hydrogen atoms. However, the determination of the accurate distribution of hydrogen atoms is difficult here. The H profile is affected by several factors, such as temperature, the accompanying defects induced by H ion irradiation, the dose of H ions, and the status of host material.

To survey the in-depth damage intuitively, SEM was used to study the cross-sectional surface of 2 MeV H^+-irradiated sample. Figure 4a clearly shows that two black bands exist, the upper one is the most damaged area, and the lower one is conjectured to be an agglomerated area resulting from H diffusion. Figure 4b shows that the most damaged area is about 30 μm deep, which is in accordance with the result of Raman investigations. Surprisingly, the lower black band appeared in SEM images at a depth about 36 μm, which is much deeper than the H ion range (around 32 μm) calculated by SRIM.

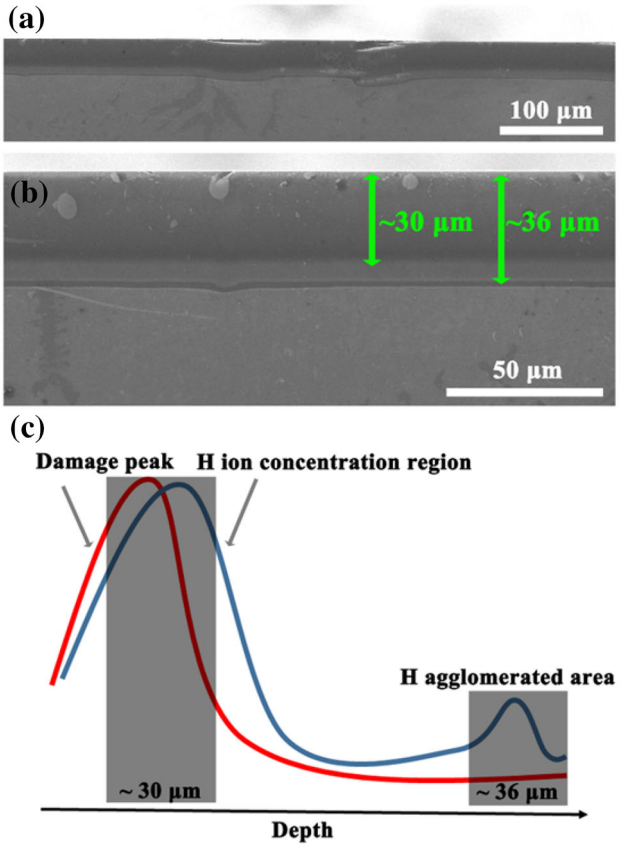

Fig. 4 (Color online) **a**, **b** SEM micrographs at 5 kV of cross section of 2 MeV H^+-irradiated sample at different magnitudes. (**c**) Schematic illustrations of the model of H diffused to the end of the area affected by H ions

We conjecture that the black band corresponds closely to the H ion-related agglomerated area. Note that this band is just at the end of the H ion-affected area. The diffusion of hydrogen may occur because the sample heats up during implantation, resulting in a possible area of H agglomeration at a depth about 36 μm. It should be pointed out that the irradiation experiment was carried out for several hours. H ion implantation induced the formation of a hydrogen- and defect-rich layer in the implanted region. The hydrogen-rich layer is slightly deeper than the defect-rich layer, shown in Fig. 1a and acts as a diffusion source during irradiation. Some hydrogen atoms reaching the ion range may begin to diffuse during the irradiation. In other words, the relatively deeper hydrogen-rich layer gives rise to the possibility that some H atoms penetrated to a deeper area, and then diffused outward and toward the sample surface. One reason that some H atoms accumulated at a depth of around 36 μm is that hydrogen atoms stop diffusing with undisturbed substrate underneath, because the diffusivity of hydrogen in our heavily irradiated n-type SiC is suppressed [11].

Furthermore, it can be seen that the damage level decreased rapidly and continuously from the most damaged region (about 30 μm) to the deepest H-affected area (about 36 μm), as shown in Fig. 3c, implying no obvious diffusion of defects produced by H implantation in the present case. This could have also been the reason why the lower black band observed in Fig. 4a, b can be ascribed to excess hydrogen diffusion, although the hydrogen atoms exhibit a tendency to interact with defects, vacancies, and self-interstitials generated during ion bombardment; acceptor and donor impurities; as well as deep-level defects and the high dose of hydrogen atoms themselves [33, 34]. The above explanation requires further confirmation.

The contrast changes in the present work are the result of an electric charge accumulation effect in SEM and are related to the conductivity of the sample surface. The areas of lower conductivity correspond to black bands in the SEM micrographs. As is generally known, secondary electron scattering is a key factor that influences SEM images. Usually, samples were covered by a thin gold layer and/or electron flooding was applied to avoid surface charging. In the present work, the accumulated negative charges on our non-conductive sample surface during SEM

tests result in a relatively dark contrast compared with more conductive specimens [35]. When the electrons bombarded the sample surface, the most damaged area and H agglomerated area deflect the impeding electrons more easily, inducing relatively lower secondary electron emission. Assuming that the polished cross sections of our samples are uniform and smooth enough, the number of secondary electrons scattered during the SEM test is closely related to the surface conductivity. Thus, the layered structures are ascribed to the differences of conductivity.

We proposed a model to explain these phenomena. Figure 4c shows a schematic illustration of the layered structures observed at the H-affected area. A black band emerges, implying this area is more resistive compared with its two sides. An electrical accumulation effect plays a role. Since the damage level, measured by Raman is rather low at the end of H-affected area (around 36 μm), we presume that some hydrogen atoms moved there, changing the electrical properties. It could happen since Laven et al. found that acceptor-like defects are created in the Si layer penetrated by the implanted protons, which may induce an inversion from n-type to p-type conductivity, influencing the diffusivity of hydrogen. And hydrogen-related excess donor appears in regions leading to an n-type inversion again [36]. These complex situations may suit for our MeV proton implantation in SiC. Hydrogen atoms will migrate within the implanted region and gradually decorate defects generated by the implantation. However, some excess hydrogens keep moving on till the end of the H-affected area. It is speculated that most of the H atoms stopped moving into the untreated substrate for the dark band still there after the samples kept for more than 6 months. Thus, this dark band can be presumed to be H agglomerated area. Appropriate test conditions are needed to observe the layered structures.

In summary, Raman measurements and the SEM micrographs in the present work reveal the damage distribution induced by MeV H ion irradiation directly. Energetic ion-induced damage over the entire ion range by studying on cross sections of SiC gives more insights into the damage effects induced by ion implantation. Further investigation of the influence of high-energy H ion-induced damage on hydrogen distribution is needed.

4 Conclusions

The damage effects in high-energy MeV H^+ implanted in SiC are studied by Raman and SEM techniques. The damage peak is slightly shallower than that predicted by SRIM. Though SRIM can give a good evaluation of the light ion-induced damage and the ion range in targets, discrepancies from the experimental results cannot be ruled out. The discrepancies can be ascribed to the errors in the simulated stopping power and energy loss calculated by SRIM. Layered structures were formed in H ion-irradiated SiC due to different contributions of damaged zone. High-energy H ions implanted in the SiC substrate result in an obvious less conductive band at the end of H ion-affected area. A charge accumulation model is proposed to elucidate the microstructures observed in this area.

References

1. J.B. Casady, R.W. Johnson, Status of silicon carbide (SiC) as a wide-bandgap semiconductor for high-temperature applications: a review. Solid State Electron. **39**, 1409–1422 (1996). https://doi.org/10.1016/0038-1101(96)00045-7
2. C. Raynaud, Silica films on silicon carbide: a review of electrical properties and device applications. J. Non-Cryst. Solids **280**, 1–31 (2001). https://doi.org/10.1016/s0022-3093(00)00350-1
3. A.A. Lebedev, A.I. VeÏnger, D.V. Davydov et al., Radiation defects in n-4H-SiC irradiated with 8-MeV protons. Semiconductors **34**, 1016–1020 (2000). https://doi.org/10.1134/1.1309411
4. N.B. Strokan, A.M. Ivanov, N.S. Savkina et al., Radiation resistance of transistor-and diode-type SiC detectors irradiated with 8-MeV protons. Semiconductors **38**, 807–811 (2004). https://doi.org/10.1134/1.1777605
5. G. Alfieri, E.V. Monakhov, B.G. Svensson, Defect energy levels in hydrogen-implanted and electron-irradiated n-type 4H silicon carbide. J. Appl. Phys. **98**, 113524 (2005). https://doi.org/10.1063/1.2139831
6. H.J. von Bardeleben, J.L. Cantin, I. Vickridge, Proton-implantation-induced defects in *n-type* 6 H-and 4 H-SiC: an electron paramagnetic resonance study. Phys. Rev. B. **62**, 10126 (2000). https://doi.org/10.1103/PhysRevB.62.10126
7. Y. Han, B.S. Li, Z.G. Wang et al., H-ion irradiation-induced annealing in He-ion implanted 4H-SiC. Chin. Phys. Lett. **34**, 012801 (2017). https://doi.org/10.1088/0256-307X/34/1/012801
8. N.B. Strokan, A.M. Ivanov, A.A. Lebedev, Transport of the charge carriers in SiC-detector structures after extreme radiation fluences. Nucl. Instrum. Meth. A. **569**, 758–763 (2006). https://doi.org/10.1016/j.nima.2006.08.077
9. H.J. von Bardeleben, J.L. Cantin, Electron paramagnetic resonance study of proton implantation induced defects in monocrystalline 4H- and 6H-SiC. Nucl. Instrum. Meth. B **186**, 201–205 (2002). https://doi.org/10.1016/S0168-583X(01)00884-9
10. A.A. Lebedev, B.Ya. Ber, G.A. Oganesyan et al., Effect of 3C-SiC irradiation with 8 MeV protons. Mater. Sci. Forum **897**, 311–314 (2017). https://doi.org/10.4028/www.scientific.net/MSF.897.311
11. N. Achtziger, J. Gillenberger, W. Witthuhn et al., Hydrogen passivation of silicon carbide by low-energy ion implantation. Appl. Phys. Lett. **73**, 945 (1998). https://doi.org/10.1063/1.122047
12. M.K. Linnarsson, J.P. Doyle, B.G. Svensson, Diffusion of hydrogen in 6H silicon carbide. Mater. Res. Soc. Symp. Proc. **423**, 625 (1996). https://doi.org/10.1557/PROC-423-62
13. J.F. Ziegler, J.P. Biersack, U. Littmarck, *The Stopping and Range of Ions in Solids* (Pergamon Press, New York, 1985)
14. H.Y. Kim, J. Kim, J.A. Freitas Jr., Penetration depth profiling of proton-irradiated 4H-SiC at 6 MeV and 8 MeV by micro-Raman

spectroscopy. Appl. Surf. Sci. **270**, 44–48 (2013). https://doi.org/10.1016/j.apsusc.2012.12.014
15. X. Wang, Y.W. Zhang, S.Y. Liu et al., Depth profiling by Raman spectroscopy of high-energy ion irradiated silicon carbide. Nucl. Instrum. Meth. B **319**, 55–61 (2014). https://doi.org/10.1016/j.nimb.2013.10.017
16. G. Guimbretière, L. Desgranges, A. Canizarès et al., Determination of in-depth damaged profile by Raman line scan in a pre-cut He^{2+} irradiated UO_2. Appl. Phys. Lett. **100**, 251914 (2012). https://doi.org/10.1063/1.4729588
17. S. Miro, G. Velisa, L. Thomé et al., Monitoring by Raman spectroscopy of the damage induced in the wake of energetic ions. J. Raman Spectrosc. **45**, 481–486 (2014). https://doi.org/10.1002/jrs.4482
18. K. Huang, Q. Jia, T.G. You et al., Defect formation in MeV H^+ implanted GaN and 4H-SiC investigated by cross-sectional Raman spectroscopy. Nucl. Instrum. Meth. B. Article in press (2017). https://doi.org/10.1016/j.nimb.2017.02.027
19. R. Devanathan, W.J. Weber, Displacement energy surface in 3C and 6H-SiC. J. Nucl. Mater. **278**, 258–265 (2000). https://doi.org/10.1016/S0022-3115(99)00266-4
20. S. Sorieul, J.M. Costantini, L. Gosmain et al., Raman spectroscopy study of heavy-ion-irradiated α-SiC. J. Phys.: Condens. Matter **18**, 5235–5251 (2006). https://doi.org/10.1088/0953-8984/18/22/022
21. J. Lindhard, V. Nielsen, M. Scharff, Approximation method in classical scattering by screened coulomb fields. Matemat. Fysis. Meddel. **36**, 1–32 (1968)
22. H.Z. Xue, Y. Zhang, Z. Zhu et al., Damage profiles and ion distribution in Pt-irradiated SiC. Nucl. Instrum. Meth. B **286**, 114–118 (2012). https://doi.org/10.1016/j.nimb.2012.02.014
23. Y. Zhang, I.T. Bae, K. Sun et al., Damage profile and ion distribution of slow heavy ions in compounds. J. Appl. Phys. **105**, 104901 (2009). https://doi.org/10.1063/1.3118582
24. K. Jin, Y. Zhang, H. Xue et al., Ion distribution and electronic stopping power for Au ions in silicon carbide. Nucl. Instrum. Meth. B **307**, 65–70 (2013). https://doi.org/10.1016/j.nimb.2013.02.051
25. C. Lan, J.M. Xue, Y. Zhang et al., Molecular dynamics simulations of ion range profiles for heavy ions in light targets. Nucl. Instrum. Meth. B **286**, 45–60 (2012). https://doi.org/10.1016/j.nimb.2012.01.020
26. S. Moll, Y. Zhang, Z. Zhu et al., Comparison between simulated and experimental Au-ion profiles implanted in nanocrystalline ceria. Nucl. Instrum. Meth. B **307**, 93–97 (2013). https://doi.org/10.1016/j.nimb.2012.12.119
27. Y. Zhang, W.J. Weber, Electronic stopping of He, B, N, and Al in SiC. Appl. Phys. Lett. **83**, 1665 (2003). https://doi.org/10.1063/1.1604473
28. Y. Zhang, W. Weber, C. Wang, Electronic stopping powers in silicon carbide. Phys. Rev. B. **69**, 205201 (2004). https://doi.org/10.1103/PhysRevB.69.205201
29. J.F. Ziegler, J.M. Manoyan, The stopping of ions in compounds. Nucl. Instrum. Meth. B **35**, 215–228 (1988). https://doi.org/10.1016/0168-583X(88)90273-X
30. Y. Zhang, T. Varga, M. Ishimaru et al., Competing effects of electronic and nuclear energy loss on microstructural evolution in ionic-covalent materials. Nucl. Instrum. Meth. B **327**, 33–43 (2014). https://doi.org/10.1016/j.nimb.2013.10.095
31. W.J. Weber, D.M. Duffy, L. Thomé, Y. Zhang, The role of electronic energy loss in ion beam modification of materials. Curr. Opin. Solid State Mater. Sci. **19**, 1–11 (2015). https://doi.org/10.1016/j.cossms.2014.09.003
32. L. Thomé, A. Debelle, F. Garrido et al., Combined effects of nuclear and electronic energy losses in solids irradiated with a dual-ion beam. Appl. Phys. Lett. **102**, 141906 (2013). https://doi.org/10.1063/1.4801518
33. M.K. Linnarsson, M.S. Janson, S. Karlsson et al., Diffusion of light elements in 4H- and 6H-SiC. Mater. Sci. Eng., B **61**, 275–280 (1999). https://doi.org/10.1016/S0921-5107(98)00517-0
34. A. Barcz, M. Kozubal, R. Jakieła et al., Diffusion and impurity segregation in hydrogen-implanted silicon carbide. J. Appl. Phys. **115**, 223710 (2014). https://doi.org/10.1063/1.4882996
35. K.H. Kim, Z. Akase, T. Suzuki et al., Charging effects on SEM/SIM contrast of metal/insulator system in various metallic coating conditions. Mater. Trans. **51**, 1080–1083 (2010). https://doi.org/10.2320/matertrans.M2010034
36. J.G. Laven, H.J. Schulze, V. Haublein et al., Dopant profiles in silicon created by MeV hydrogen implantation: influence of annealing parameters. Phys. Status Solidi C **8**, 697–700 (2011). https://doi.org/10.1002/pssc.201000161